Rossby Waves and Zonal Flux Anomalies in the Analogs of Hadley and Ferrell Cells of the General Atmospheric Circulation: Model and Experiments[1]

A. E. Gledzer[a], E. B. Gledzer[a], A. A. Khapaev[a], and O. G. Chkhetiani[a], *, *

[a] *Obukhov Institute of Atmospheric Physics, Russian Academy of Sciences, Moscow, 119017 Russia*
*e-mail: lgg@ifaran.ru
**e-mail: ochkheti@ifaran.ru

Abstract—Numerical and laboratory experiments have been carried out to study the intrusion of anomalies into the axisymmetric distribution of the velocity field generated by sink sources and the MHD method in a rotating circular channel with a sloping bottom. A sectoral decrease in the intensity of the external force in a certain range of values has a decelerating effect on the velocity of propagation of anticyclones through the channel, while it has almost no influence on the dynamics of cyclones. At the same time, a significant part of moving anticyclones can disappear or almost stop, or new quasi-stationary anticyclones appear, despite there being no notable changes in the visible pattern of eddy propagation in the channel in the sector in which external intervention had been performed. However, changes are notable over the entire channel or in its individual parts in the mean characteristics of the eddy field. These anomalies can be interpreted as a decrease in the intensity of the subtropical Hadley cell, which is accompanied by a weakening of the trade winds in a sector of the equatorial atmospheric circulation and a decrease in the westerly transport at midlatitudes. The state of the mixture of standing and moving eddies is considered on the basis of a simple analytical model of the resonant interaction of transient (with an intermediate velocity maximum) modes in a shear flow. In this case, the amplitude of the stationary background state has the same dependence on the β effect as in the well-known Sverdrup relation for the stream function of the surface current in the ocean basin in the studies of the western boundary current intensification.

Keywords: general circulation anomalies, Hadley and Ferrel cells, blocking, resonance interaction, Rossby waves, transient instability, annular channel, sources and sinks, shallow-water equations, MHD experiments

DOI: 10.1134/S0001433823040072

1. INTRODUCTION

The atmosphere, based on the known scheme of zonal mean circulation, consists of cells with various meridional and zonal flows: Hadley, Ferrell, and polar (Lorenz, 1970; Matveev, 2000; Mohanakumar, 2011). Such an axisymmetric circulation pattern is the main (basic state) for the application of various numerical and analytical methods for studying baroclinic or barotropic (shear) instabilities developing in the corresponding hydrodynamic flows, which lead to the formation of nonaxisymmetric flows (the Rossby regime) (Antar and Fowlis, 1981). It is important, however, that the violation of the axial symmetry of the mentioned cells is largely due to the distribution of surface and thermal contrasts over the continents (Cook, 2003).

It is interesting to consider the effect of longitudinal anomalies on the generation and distribution of Rossby waves in the case of asymmetric distribution of velocity fields in the Hadley and Ferrel cells. We use the results of both laboratory and numerical experiments with shallow water equations.

Rossby waves are known to be an important contribution to the general circulation of the atmosphere. In extratropical zones, the propagation velocity of these waves to the west $\dfrac{\beta}{k_x^2 + k_y^2 + \dfrac{1}{L_0^2}}$ (k_x and k_y are zonal (azimuth) and meridional wave numbers, and L_0 is the Rossby deformation radius) with respect to the mean transport decreases along with the latitudinal φ variation in the Coriolis parameter $f = 2\Omega \sin \varphi$

---

[1] This paper was prepared on the basis of an oral presentation at the IV All-Russian Conference with international participation "Turbulence, Atmospheric and Climate Dynamics" dedicated to the memory of Academician A.M. Obukhov (Moscow, November 22–24, 2022).
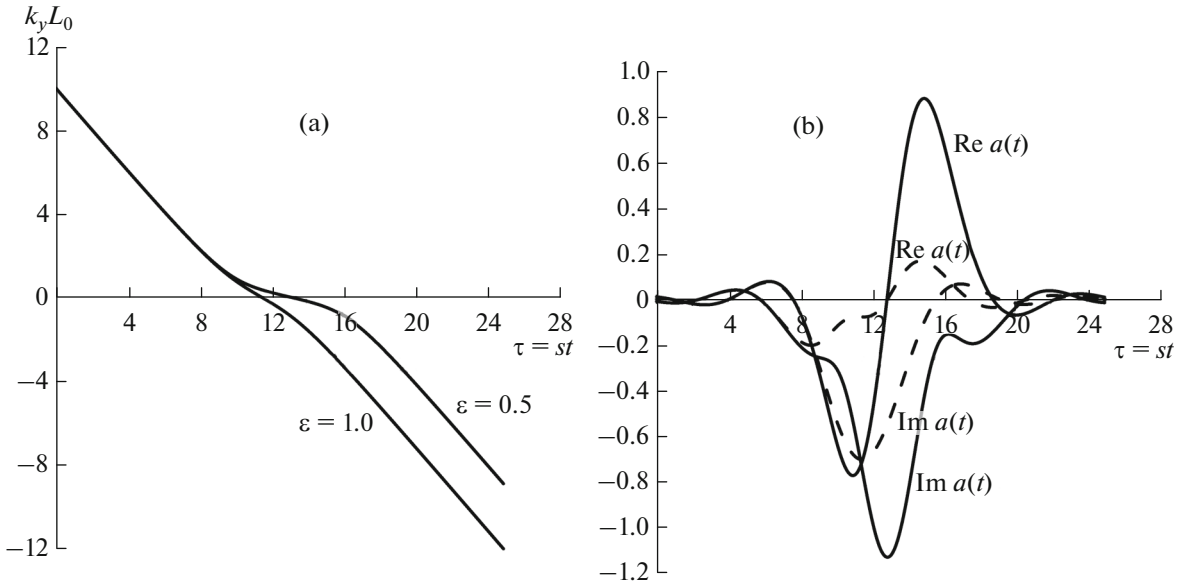
Fig. 1. (a) Dependence of meridional wave number $k_y L_0$ on τ for values $\varepsilon = 0.5$, $\varepsilon = 1.0$, and $\varepsilon = k_x L_0$. (b) Dependence of amplitude $a(t)$ on τ for values $\varepsilon = 0.5$ (solid curves) and $\varepsilon = 1.0$ (dashed line).

($\beta = 2\Omega/R\cos\varphi$, R is the radius of the planet). One important source of Rossby wave generation is the shear instability of hydrodynamic flows in the extratropical zone (eastward polar transport and westward flow at midlatitudes). Among the large number of approaches and solutions for shear hydrodynamic instability with the β effect, the simplest are the explicit formulas describing the solutions of the Charney–Obukhov equations (Obukhov, 1949; Dolzhansky, 2011) for stream function ψ with time-dependent meridional wavenumber $k_y = k_y(t)$ (transient instability) (Chagelishvili and Chkhetiani, 1995; Chkhetiani et al., 2015; Chkhetiani and Kalashnik, 2018):

$$\psi = a(t)e^{i\left(k_x x + k_y(t)y\right)} + \psi_0, \quad \psi_0 = -Uy - s\frac{y^2}{2},$$

$$\frac{\partial}{\partial t}\left(\Delta\psi - \frac{1}{L_0^2}\psi\right) + [\psi, \Delta\psi] + \beta\frac{\partial\psi}{\partial x} = 0, \quad u = -\frac{\partial\psi}{\partial y}, \quad (1)$$

$$v = \frac{\partial\psi}{\partial x},$$

$$\left(k^2 + \frac{1}{L_0^2}\right)\frac{dk_y(t)}{dt} + sk^2 k_x = 0, \quad k^2(t) = k_x^2 + k_y^2(t),$$

$$\frac{d}{dt}\left[\left(k^2 + \frac{1}{L_0^2}\right)a\right] - ik_x\left(\beta - k^2 U\right)a = 0, \quad (2)$$

where U and s are the background velocity and horizontal shear of velocity, respectively, with initial conditions $k_{0y} \gg k_x$ (the condition of instability of long waves for the Kolmogorov flow (Meshalkin and Sinai, 1961; Gledzer et al., 1981)); $a(t = 0) = a_0$.

Formulas with wavenumber versus time dependence were used to find unstable solutions in the flows with elliptical streamlines (Gledzer and Ponomarev, 1992), in dynamical systems (Shukhman, 2005), or for the Hadley circulation with a horizontally inhomogeneous temperature distribution (Gledzer, 2008).

Solutions of Eqs. (2) show (Chkhetiani and Kalashnik, 2018) that, under the condition of long waves $L_v \gg L_0$, $k_x = \frac{2\pi}{L_v}$, there are comparatively long time intervals Δt, during which meridional wavenumber $k_y(t)$, depending only on shear s (at fixed k_x, L_0), changes only slightly (step) and $|k_y(t)| \ll k_x$ (see Fig. 1a). The wave energy proportional to $|a(t)|^2$ increases from small initial values and remains quasistationary during the same time interval Δt (intermediate (transient) velocity maximum). This case is shown in Fig. 1a for $k_x = \frac{\varepsilon}{L_0}$ at $\varepsilon = 0.5$. If $\varepsilon = 1$ (Fig. 1a), i.e., $L_v = 2\pi L_0$, then $k_y(t)$ decreases monotonously; however, for $|k_y| \le k_x$, the amplitude of $|a|$ also strongly increases (Fig. 1b).

2. RESONANT INTERACTION OF TRANSIENT MODES

We will consider Eqs. (1) and (2) as a mechanism for generating Rossby waves with a meridional wave number $k_y \ne 0$, formed in the previously indicated

interval Δt, with an amplitude in the vicinity of its maximum values

$$|a| = a_0 \frac{k_x^2 + k_{0y}^2 + \frac{1}{L_0^2}}{k_x^2 + k_y^2 + \frac{1}{L_0^2}} \gg |a_0|$$

at $k_y^2 \ll k_{0y}^2$, $k_y^2 \ll k_x^2$.

If there are two waves with zonal wave numbers k_x and $2k_x$ and the same meridional number k_y, then there is the same frequency for them ω calculated from the Rossby formula,

$$\omega = -\frac{\beta k_x}{k_x^2 + k_y^2 + \frac{1}{L_0^2}} = -\frac{\beta 2k_x}{(2k_x)^2 + k_y^2 + \frac{1}{L_0^2}},$$

under condition

$$2k_x^2 = k_y^2 + \frac{1}{L_0^2}. \tag{3}$$

Relation (3), which is necessary for the search for a stationary wave, includes the Rossby deformation radius L_0. Another condition that determines the relationship between k_x and k_y, can be setting the relief as a natural factor that determines the scale of the Rossby waves. In particular, taking into account the shape of the relief, which is similar to the horizontal velocity shear s in Eqs. (2), gives the second relationship between k_x and k_y, as a result of which these wave numbers can be specified.

During the resonant interaction of these two waves, formation of quasi-stationary wave $e^{ik_x x}$, independent of coordinate y, with wavenumber k_x is possible:

$$\begin{aligned}\psi = {}&A(t)e^{ik_x x} + B(t)e^{i(k_x x + k_y y - \omega t)} \\ &+ C(t)e^{i(2k_x x + k_y y - \omega t)} + c.c.\end{aligned} \tag{4}$$

We use the standard procedure with complex coefficients A, B, and C with averaging over oscillations with frequencies multiple to ω, and obtain the following equations:

$$\begin{aligned}\left(k_x^2 + \frac{1}{L_0^2}\right)\dot{A} &= 3k_x^3 k_y B^* C + ik_x \beta A, \\ \left(k_x^2 + k_y^2 + \frac{1}{L_0^2}\right)\dot{B} &= -\left(3k_x^2 + k_y^2\right)k_x k_y A^* C, \\ \left(4k_x^2 + k_y^2 + \frac{1}{L_0^2}\right)\dot{C} &= k_y^3 k_x AB\end{aligned} \tag{5}$$

with energy integrals $E = F(1)$ and squarred vorticity $\Omega^2 = F(2)$:

$$\begin{aligned}F(n) = {}&\left(k_x^2 + \frac{1}{L_0^2}\right)^n |A|^2 + \left(k_x^2 + k_y^2 + \frac{1}{L_0^2}\right)^n |B|^2 \\ &+ \left(4k_x^2 + k_y^2 + \frac{1}{L_0^2}\right)^n |C|^2.\end{aligned}$$

Equations (5) are a particular case of the triplet interaction of waves, in which the time frequency of one of the waves is equal to zero. However, waves with amplitudes B and C in (4) form three-mode blocks of interactions with waves $e^{\pm i(3k_x x + 2k_y y - 2\omega t)}$, $e^{\pm i(4k_x x + 2k_y y - 2\omega t)}$ with amplitudes $\sim |BC|$, $|C|^2$, which contain only time-oscillating modes. These blocks, according to the ideas of resonant interaction, give corrections of the following orders, which disappear for stationary waves in the framework of the three-mode theory due to time averaging.

It is worth noting that, during interaction, the modes $e^{\pm i(3k_x x + 2k_y y - 2\omega t)}$, $e^{\pm i(4k_x x + 2k_y y - 2\omega t)}$ with amplitudes $\sim |BC|$, $|C|^2$ can give fourth-order corrections $\sim |BC||C|^2$ for stationary state $\sim e^{ik_x x}$. They can be considered small under conditions of relatively small amplitudes B, C. This condition is used below to solve Eqs. (5). In any case, if we take into account a large number of three-mode interactions, the main, initial (the topmost in the hierarchy of triplets) ones are Eqs. (5).

The term with coefficient β (β effect) in the first equation (5) and the finite amplitude B, C of the Rossby waves leads to the solution of Eqs. (5) with a stationary amplitude $A(t) = A_0 = \text{const}$ of the zonal component of the stream function ψ.

We assume that such a value $A(t) = A_0$ exists, i.e., in the second and third equations (5) $A^*(t) = A_0^*$, $A(t) = A_0$. From these equations we get a solution for B and C:

$$B(t) = B_s \sin(\nu t) + B_c \cos(\nu t),$$

$$C(t) = -\frac{\left(k_x^2 + k_y^2 + \frac{1}{L_0^2}\right)}{\left(3k_x^2 + k_y^2\right)k_x k_y} \frac{\nu}{A_0^*}\left(B_s \cos(\nu t) - B_c \sin(\nu t)\right), \tag{6}$$

$$\nu = k_y^2 |A_0|\mu,$$

$$\mu = \sqrt{\frac{k_x^2\left(3k_x^2 + k_y^2\right)}{\left(k_x^2 + k_y^2 + \frac{1}{L_0^2}\right)\left(4k_x^2 + k_y^2 + \frac{1}{L_0^2}\right)}}. \tag{7}$$

Then, using B^*C (without oscillation terms $\sim\sim \sin(2\nu t)$, $\cos(2\nu t)$) in the first equation (5), we obtain $A_0 = A_0^*$ as a zero approximation and

$$A_0 = \frac{3}{2}\frac{k_x k_y^2}{\beta}\mu_0 eB^2, \quad eB^2 = \mathrm{Im}\left(B_c^* B_s - B_c B_s^*\right),$$

$$e = \pm 1, \quad \mu_0 = \mu\frac{k_x^2 + k_y^2 + \dfrac{1}{L_0^2}}{3k_x^2 + k_y^2}. \tag{8}$$

Taking into account that A_0 is a real value, the formula for C in (6) will be written as

$$C(t) = -\mu_c\left(B_s \cos(\nu t) - B_c \sin(\nu t)\right),$$
$$\mu_c = k_y \mu_0 / k_x. \tag{9}$$

At $t = 0$, we get initial conditions from (6) and (9): $B_c = B(0)$, $B_s = -\dfrac{1}{\mu_c}C(0)$.

Wave $\psi_0 = A_0\left(e^{ik_x x} + e^{-ik_x x}\right) = 2A_0 \cos(k_x x)$ corresponds to the stationary (background) distribution pattern of the stream function over zones with vorticity of different signs $\Delta\psi_0 = -2k_x^2 A_0 \cos(k_x x)$. However, this background distribution exactly produces the nonstationary part as the next approximation (which is obtained if we take into account the oscillation terms discarded above under the condition that A_1 and A_2 are relatively small compared to A_0):

$$A(t) = A_0 + A_1(t) + iA_2(t),$$

$$A_1 = \frac{1}{2}N\left(d_s \cos(2\nu t) - d_c \sin(2\nu t)\right), \tag{10}$$

$$A_2 = \frac{1}{2}\frac{N^2}{A_0}\left(d_s \sin(2\nu t) + d_c \cos(2\nu t)\right),$$

$$N = \beta\frac{1}{k_x k_y^2}\frac{1}{\mu}\frac{k_x^2}{k_x^2 + \dfrac{1}{L_0^2}}, \quad d_s = \frac{|B_s|^2 - |B_c|^2}{eB^2},$$

$$d_c = \frac{B_c^* B_s + B_c B_s^*}{eB^2}. \tag{11}$$

It follows from (8) that the background component of ψ_0 exists if $B^2 = \left|\mathrm{Im}\left(B_c^* B_s - B_c B_s^*\right)\right| \neq 0$, i.e., not under all initial conditions for the Rossby wave amplitudes $B(0)$, $C(0)$. In addition, solutions (10) are obtained under the conditions $N|d_s| \ll |A_0|$, $N|d_c| \ll |A_0|$, which also imposes a number of conditions on the parameters in (11).

Formulas (10) show that periodic oscillations with frequency $2\nu = 2k_y^2 A_0 \mu$ equal to the spatial period of the stationary wave $L = 2\pi/k_x$ are superimposed on the background stationary circulation $L = 2\pi/k_x$. In addition, Rossby waves $B(t)e^{i\left(k_x x + k_y y - \omega t\right)}$, $C(t)e^{i\left(2k_x x + k_y y - \omega t\right)}$ are also modified by time oscillations according to (6), (10) with frequency ν, which leads to oscillations with frequencies $\omega \pm \nu$ or zonal transport with velocities

$\dfrac{\omega \pm \nu}{k_x}$ depending on the amplitude $|A_0|$ of the stationary component of the flow.

The appearance of parameter β in the denominator of the expression for amplitude A_0 (8) is a feature of the background stationary field $\psi_0 = 2A_0 \cos k_x x$. The well-known Sverdrup relation for the stream function of the surface current in the ocean basin in the study of the western boundary intensification of currents (R is the radius of the Earth, φ is the latitude, λ is the longitude, and H is the characteristic depth) has the same dependence on β (Sverdrup, 1947; *Okeanologiya*, 1978).

$$\frac{1}{R\cos\varphi}\frac{\partial\psi}{\partial\lambda} = \frac{\mathrm{rot}_z\bar{\tau}/H}{\beta}. \tag{12}$$

In this relation, the vertical component of the rotor of friction stress caused by surface waves of wind circulation over the ocean (for example, the Atlantic) is the coefficient at $\dfrac{1}{\beta}$: $\tau_\lambda = \langle u'w'\rangle$; $\tau_\varphi = \langle v'w'\rangle$ is the quadratic form, where u', v', and w' are the velocity fluctuations of surface waves generated by the wind (the dimension of the function of total fluxes φ in (12) is m³/s). In case (8), the coefficient at $\dfrac{1}{\beta}$ includes a quadratic form associated with Rossby waves.

The dimension of A_0, A_1, A_2, N, B_s, B_c, B, as well as stream functions ψ, ψ_0, is m²/s. Let us estimate the orders of magnitude assuming $k_y \sim k_x \sim \dfrac{1}{L_0}$ (this corresponds to Eq. (3)). We assume for the amplitude of the velocity of the background stationary flow ψ_0 that $V_a \equiv 2|A_0|k_x$; the amplitude of the velocity of the background stationary flow in (5) is $V_R = |B|k_x$. We get from (3) that $|A_0| = \dfrac{3}{2}\dfrac{k_x k_y^2}{\beta}\mu_0 B^2 = \dfrac{3}{2}\dfrac{k_x k_y^2}{\beta}\mu_0\dfrac{V_R^2}{k_x^2}$.

Hence, $V_a = 3\dfrac{k_y^2}{\beta}\mu_0 V_R^2$, or at $V_a = V_R$, $V_R = \dfrac{\beta}{3k_y^2\mu_0} \sim$ $L_0^2\beta \sim 10$ m/s at $L_0 \sim 10^6$ m, $\beta \sim 10^{-11}$ (m⁻¹ s⁻¹).

As was previously noted, wave $\psi_0 = 2A_0 \cos(k_x x)$ forms vorticity anomalies with a scale of $L_x = \dfrac{2\pi}{k_x}$ along coordinate x (longitude). In laboratory and numerical experiments simulating surface air flows in the tropical and polar Hadley and Farrell cells at midlatitudes, such anomalies can be reproduced if the symmetry of the currents in the analogues of the mentioned cells is broken—Eqs. (5) are invariant under substitutions $A \to Ae^{i\varphi_a}$, $B \to Be^{i\varphi_b}$, $C \to Ce^{i\varphi_c}$, $\varphi_c = \varphi_a + \varphi_b$.
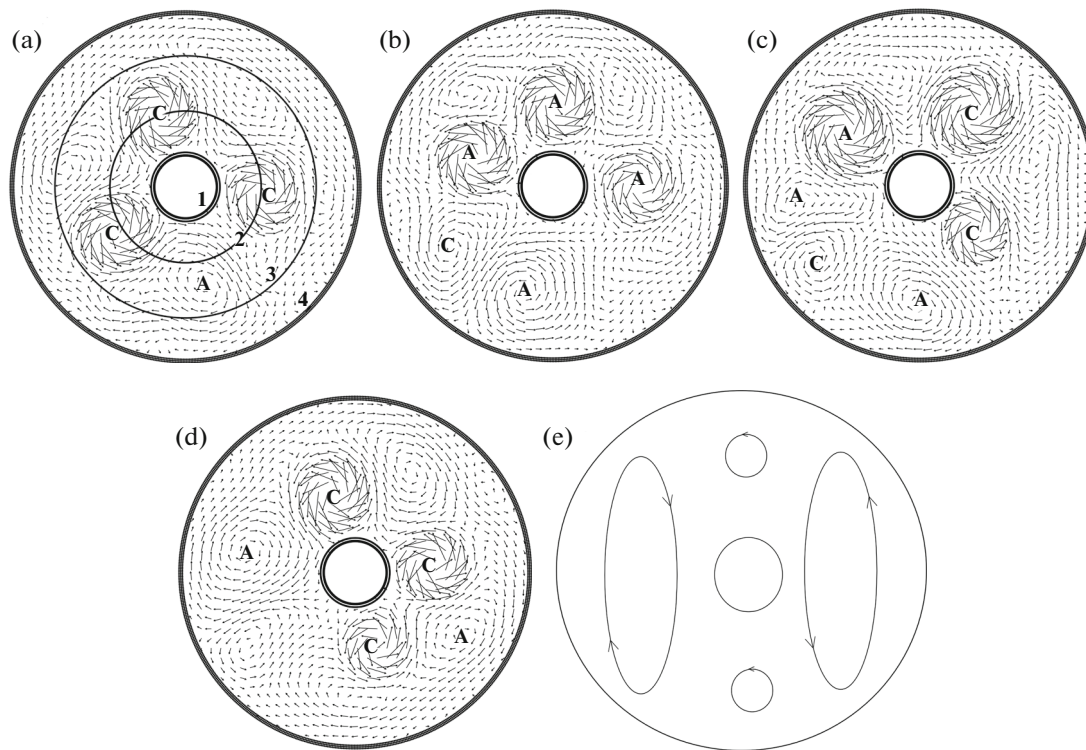
Fig. 2. (a−d) Velocity field vectors for the numerical experiment with sources ($E = 0.8$) and sinks ($E = -0.8$), T = 6 s, C is a cyclone, and A is an anticyclone; (e) schematic of the superposition of Rossby waves with wavenumbers differing by a factor of two.

3. NUMERICAL EXPERIMENTS

Numerical experiments were performed for the flows in thin layers of fluid in an annular rotating (counterclockwise rotation: North Pole) channel based on shallow water equations; the β effect was modeled by an inclined bottom (Dolzhansky, 2011). The equations and calculation methods were presented in detail in a number of works (Gledzer, 2014, 2015; Gledzer et al., 2018, 2021).

The source−sink method was used for the purposes of this work to generate eddy motions in a rotating channel. To simulate subtropical and polar easterly winds and western transport at midlatitudes (three-flow configuration), sources−sinks of fluid were used in thin annular layers on the inner (1) and outer (4) boundaries of the channel and two layers (2) and (3) in its middle. These source−sink layers are shown in Figs. 2a–2d by circles: 1 and 3 are sources and 2 and 4 are sinks. In arbitrary units (Gledzer et al., 2021), the power of sources (1 and 3) is $E = 0.8$, and the power of sinks (2 and 4) is $E = -0.8$. The sources of layer 1 induce a directional flow towards the sink in layer 2. This flow is deflected by the Coriolis force to the right of it (clockwise between layers 1 and 2). This corresponds to the eastern winds. It is similar for the flow from source 3 to sink 4. The flow from source 3 to sink 2 forms a counterclockwise Coriolis motion in the ring between 2 and 3. This is analogous to the westward transport at midlatitudes.

This configuration of flows forms velocity shears in the channel, which, as a result of instability, lead to the appearance of cyclonic (C) (Fig. 2) with counterclockwise rotation and anticyclonic (A) eddies (in Figs. 2a, 2b, 2c, and 2d, the angular velocity of rotation channel is $\Omega = \dfrac{2\pi}{T}, T = 6$ s). This entire system of eddies moves clockwise, i.e., propagates westward in accordance with the concept of Rossby waves (in the Northern Hemisphere).

However, the system of eddies that appears is not symmetrical: three closely located cyclones exist almost in half of the channel (Figs. 2a, 2b), and the other half is occupied by an anomaly, which contains an extensive anticyclone (Figs. 2a, 2b) (or two, Fig. 2c) and sometimes a cyclone (Figs. 2b, 2c).

The schematic pattern of the velocity field in Fig. 2 can be roughly represented as a superposition of two Rossby waves with wavenumbers ($m = 2$, $m = 4$) in longitude (Fig. 2e) that differ by a factor of two. In this case, wave $m = 2$ intensifies the cyclonic circulation of wave $m = 4$ in one half of the channel and the anticyclonic circulation in the other. The angular velocities of these two waves probably differ, since the motion to the west is not quite uniform (the time interval between the patterns in Figs. 2a–2d is the same, $\Delta\tau = 200$, $\tau = \Omega t$).

Figure 3 shows the dependences of the azimuthal (longitude) $0 \leq \lambda \leq 2\pi$ coordinates of the centers of
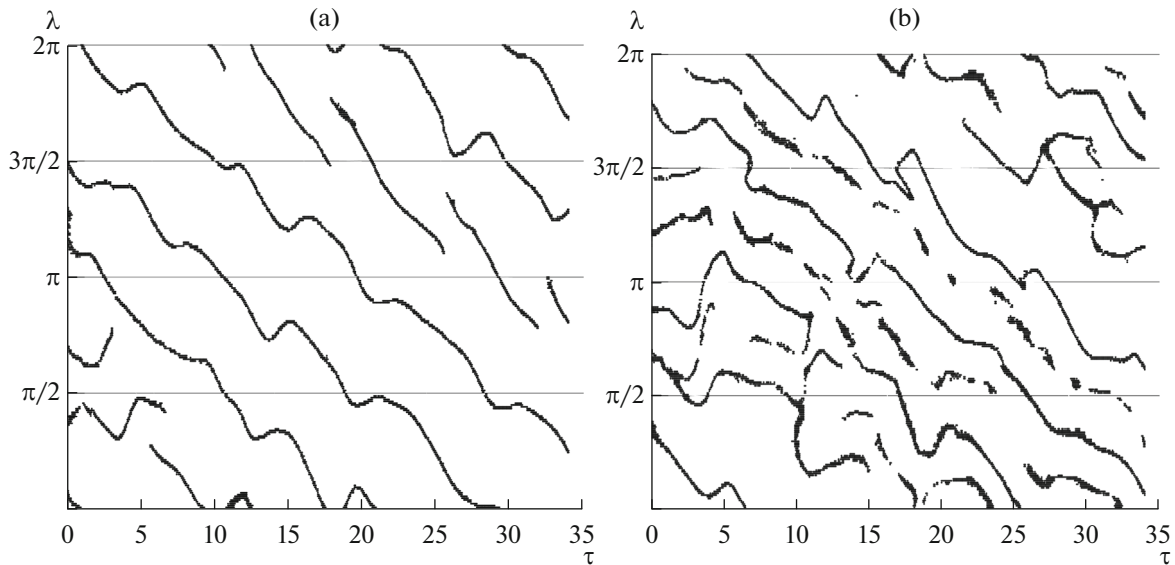
Fig. 3. Time evolution of $\tau = t/T$ (period $T = 6$ s) of the azimuthal angular coordinates λ of the centers of cyclones (a) and anticyclones (b) in numerical experiments with sources ($E = 0.8$) and sinks ($E = -0.8$) in a three-flow configuration. The slope to the right (decrease in λ) corresponds to the clockwise motion of the eddies (Fig. 2).

cyclones (Fig. 3a) and anticyclones (Fig. 3b) for moving eddies (Fig. 2). The centers are determined by the velocity field as a point in the nearest neighborhood of which the azimuthal and meridional velocity components change sign. Since cyclonic eddies are more intense, anticyclones moving at a different angular velocity (the mean slopes of the lines in Fig. 3b for anticyclones are smaller than in Fig. 3a for cyclones) sometimes change their position or completely disappear; as a result, the lines of anticyclone centers become discontinuous. However, in general, the angle λ for almost all anticyclones in Fig. 3b decreases, like for cyclones (clockwise motion).

In the case shown in Fig. 2, anomalies appear as a result of the dynamics of the eddy system. It is interesting to consider the influence of an externally introduced anomaly on the distribution of western and eastern flows in the channel. We assume that, in the lower quarter of the channel $\frac{3\pi}{2} - \frac{\pi}{4} < \lambda < \frac{3\pi}{2} + \frac{\pi}{4}$ (Fig. 4a), the sources−sinks in the annular layers decreased their intensity by half: instead of $E = \pm 0.8$, there is an inflow−outflow $E = \pm 0.4$. Due to the inflows−outflows in other parts of the layers, the velocity field in this quarter of the channel does not necessarily decrease by half, although it may lose the original symmetry of the main flow.

This anomaly can be interpreted as a decrease in the intensity of the subtropical Hadley cell, which is accompanied by a weakening of the trade winds in some sector of the equatorial atmospheric circulation and a decrease in the westerly transport at midlatitudes.

Velocity fields for the indicated inflows−outflows $E = \pm 0.8$, $E = \pm 0.4$, which only slightly differ from Fig. 2, are shown in Fig. 4a for some time moments when there was no external anomaly in the distribution of sources−sinks. It is possible that, only at some moments of time, four cyclones (instead of three) of high intensity appeared more clearly, as in the second of Fig. 4a. The lines of cyclone centers shown in Figs. 4b do not strongly differ compared to Fig. 3a.

However, the lines of the centers of anticyclones (Fig. 4c), while retaining the same broken structure as in Fig. 3b, has almost lost the average slope to the right; i.e., angle λ does not decrease on average. Actually, this is stationaring, and the external anomaly at $\frac{3\pi}{2} - \frac{\pi}{4} < \lambda < \frac{3\pi}{2} + \frac{\pi}{4}$ slows down only the anticyclones—only some lines of those anticyclone centers shown in Fig. 4c have a significant mean slope to the right: at some moments of time they move clockwise together with cyclones (Fig. 4b).

It is worth noting that, with an increase in the externally induced circulation anomaly, cyclones can also stop, forming correlated structures with anticyclones. In particular, this was observed in a numerical experiment with the absence of inflow−outflow ($E = 0$) in the lower quarter of the channel $\frac{3\pi}{2} - \frac{\pi}{4} < \lambda < \frac{3\pi}{2} + \frac{\pi}{4}$ with the previous value $E = \pm 0.8$ for the other angles λ. The patterns of the lines of the centers of cyclones and anticyclones turned out to be on average horizontal and qualitatively similar (differing only in the values of the angles λ).
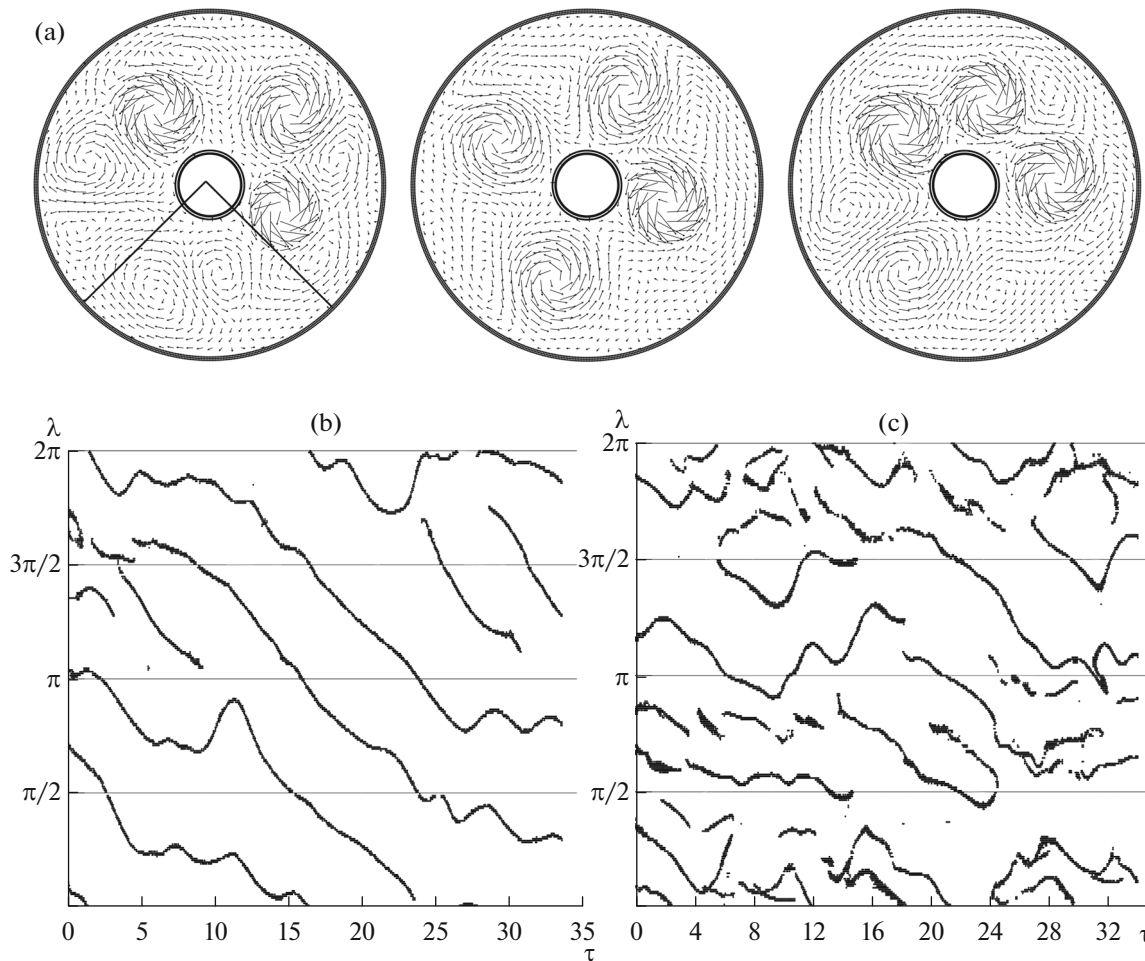
Fig. 4. (a) Velocity field vectors in a numerical experiment in a three-flow configuration with sources–sinks ($E = \pm 0.8$) in the upper three quarters of the channel $2\pi - \frac{\pi}{4} < \lambda < 2\pi$, $0 < \lambda < \pi + \frac{\pi}{4}$ and sources–sinks ($E = \pm 0.4$) in the lower quarter of the channel $\frac{3\pi}{2} - \frac{\pi}{4} < \lambda < \frac{3\pi}{2} + \frac{\pi}{4}$ (b, c) time evolution of $\tau = t/T$ (period $T = 6$ s) of the azimuthal angular coordinates λ of the centers of cyclones (b) and anticyclones (c) in numerical experiments with sources and sinks $E = \pm 0.8$, $E = \pm 0.4$.

The same decelerating effect for anticyclones is shown in a numerical experiment in a different configuration, when only the western transport at midlatitudes and the eastern one at southern latitudes are simulated (two-flow configuration). To do this, instead of the source sink in the annular layers 2, 3 (Fig. 2a), a source was placed in a circle between them. The power of sinks in the inner annular layer 1 was $E_1 = 0.2$, on the outer layer 3 it was $E_3 = 0.5$, and the power of the source was calculated from the mass conservation condition.

Figures 5a and 5b show the lines of centers of cyclones and anticyclones without a source–sink anomaly in sector $\frac{3\pi}{2} - \frac{\pi}{4} < \lambda < \frac{3\pi}{2} + \frac{\pi}{4}$. In this case, the lines of cyclones and anticyclones do not differ much; on average they are inclined to the right and

describe the clockwise motion along the channel. One peculiarity of the dynamics shown in Figs. 5a and 5b is a two-mode motion: until some time $t_{cr} \sim T \times 30$, there was one mode of motion of the centers, which was, after t_{cr}, replaced by a slower motion of cyclones and anticyclones. The work (Gledzer et al., 2021) was devoted to the multimode regime in numerical and laboratory experiments. The difference of the dynamics shown in Figs. 5a and 5b from that in (Gledzer et al., 2021) is the invariance of the external parameters in the numerical experiment.

The differences between the lines of the centers of cyclones and anticyclones are observed if the power of sources–sinks in the anomaly sector $\frac{3\pi}{2} - \frac{\pi}{4} < \lambda < \frac{3\pi}{2} + \frac{\pi}{4}$ is zero $E_1 = E_3 = 0$ (Figs. 5c, 5d). In this case,
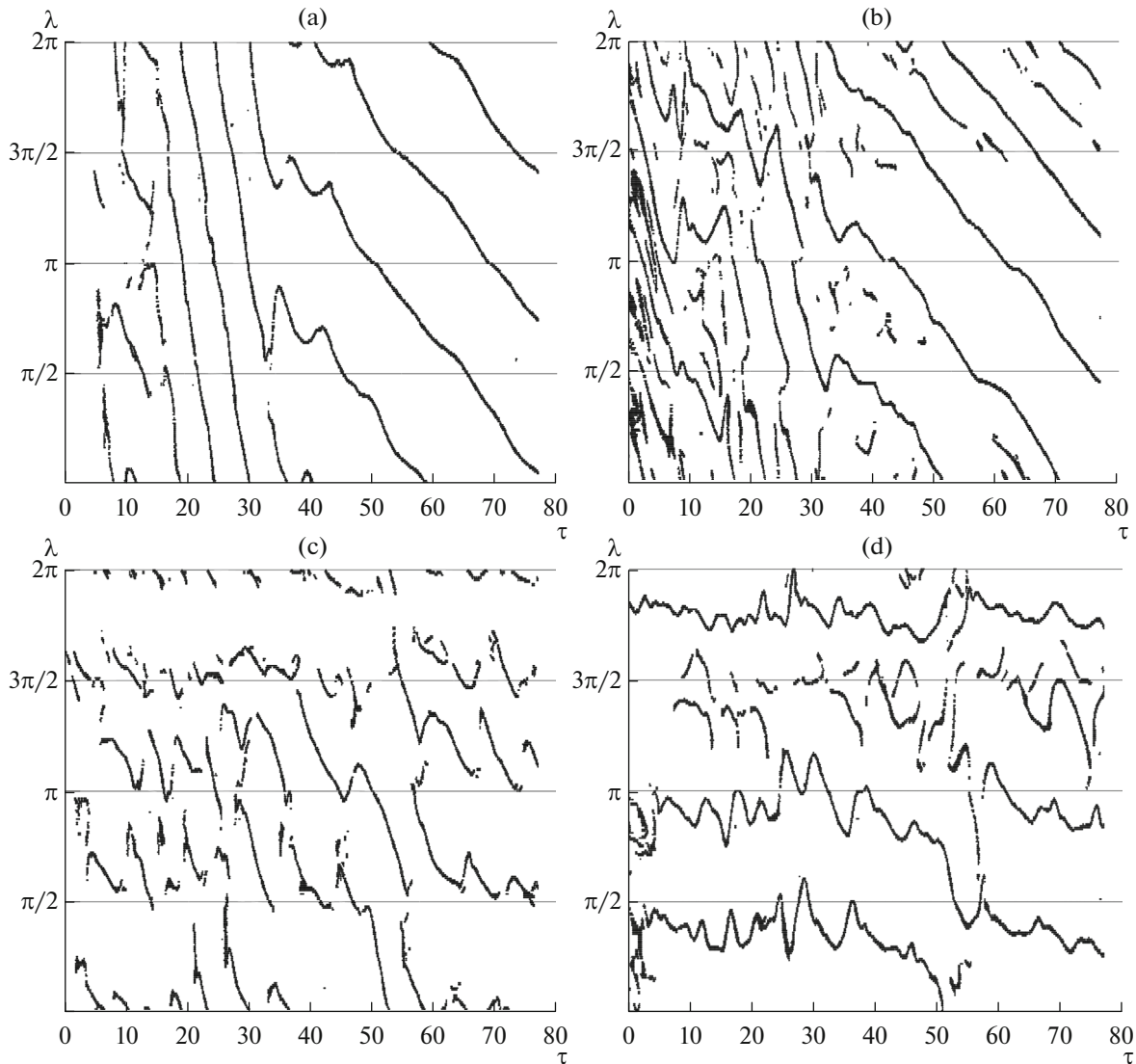
Fig. 5. Time evolution of $\tau = t/T$ of the azimuthal angular coordinates λ of the centers of cyclones (a, c) and anticyclones (b, d) in numerical experiments with two-flow configuration: (a, b) $E_1 = 0.2$, $E_2 = 0.5$; (c, d) $E_1 = 0$, $E_2 = 0$.

the broken structure of the lines is enhanced, but, like in Fig. 4c, most of the anticyclone lines are generally horizontal; anticyclones, on average, do not change their azimuthal position. Cyclones (Fig. 5c) mostly continue moving along the channel, although their lifetime has decreased in comparison with the nonanomalous case in Fig. 5a due to uncoordinated motion with anticyclones.

Numerical experiments show that sectoral anomalies can affect the mean characteristics of the vorticity field in the channel. Figure 6 shows the vorticity differences $\Delta\Omega$ between the anomalous and nonanomalous cases (for a three-flow configuration) averaged over the rings between the sources–sinks on circles 2 and 3 (Fig. 6a) and 3 and 4 (Fig. 6b). In the ring between layers 2 and 3, the presence of an anomaly

slightly increased the positive vorticity (Fig. 6a), which means an increase in the cyclonic component. In the ring between layers 3 and 4 (Fig. 6b), on the contrary, the change in vorticity became mostly negative. This corresponds to the strengthening of anticyclonic tendencies in this part of the stream.

4. LABORATORY EXPERIMENTS

Laboratory experiments were carried out using the Magnetohydrodynamic (MHD) method for generating flows in a rotating annular channel filled with a conducting liquid. The experimental setup and experimental technique have been presented in detail in a number of works (Gledzer et al., 2013, 2018, 2021).
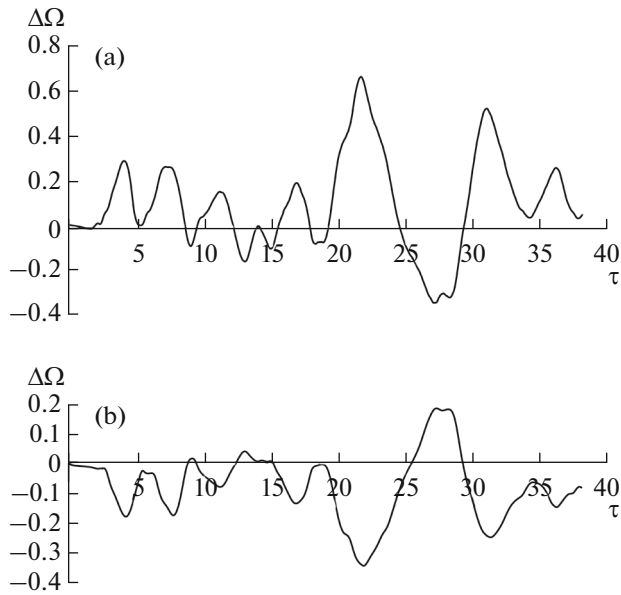
Fig. 6. Differences in the vorticity between the anomalous and nonanomalous cases (for a three-flow configuration) averaged over the rings between the sources–sinks on circles 2 and 3 (a) and 3 and 4 (b) (see Fig. 2a).

Fig. 7. Scheme of layout of electrodes 2, 1, and 3; permanent magnets; and division into sectors I–IV in Figs. 9 and 10 in the channel of the laboratory setup.

The experiments simulate the situation in the Southern Hemisphere with the channel rotating clockwise.

In the MHD approach, the flows are generated by the interaction of the magnetic field of permanent magnets (neodymium, 0.36 T and ferrite, 0.175 T) placed along three (or two) circles (Fig. 7) under a bottom inclined from the center to the periphery in the channel, and a radially directed current between electrodes 1 and 2 on the outer and inner boundaries with radii of 5 cm and 36 cm. A number of the magnets on the outer circle were replaced with ferrite magnets or removed altogether (hereinafter, experiment 1, Figs. 11a–11f). In experiments with the results shown in Figs. 11aa and 11bb, on the contrary, a line of magnets was removed from the middle circle (experiment 2).

Radially directed current $\vec{j}$ and vertically directed field $\vec{H}$ form the Ampère force in a direction normal to them $\sim\left[\vec{j}, \vec{H}\right]$, acting on a conductive liquid (10% solution of $CuSo_4$) above an inclined bottom. The directions of the magnetic field (with different poles along the circles) and the electric current between electrodes 1 and 2 are chosen to induce a flow directed to the east in the middle of the channel (western transport at midlatitudes), while in the inner and outer parts of the channel they induce flows directed to west (trade winds at the outer border of the channel and the eastern polar wind).

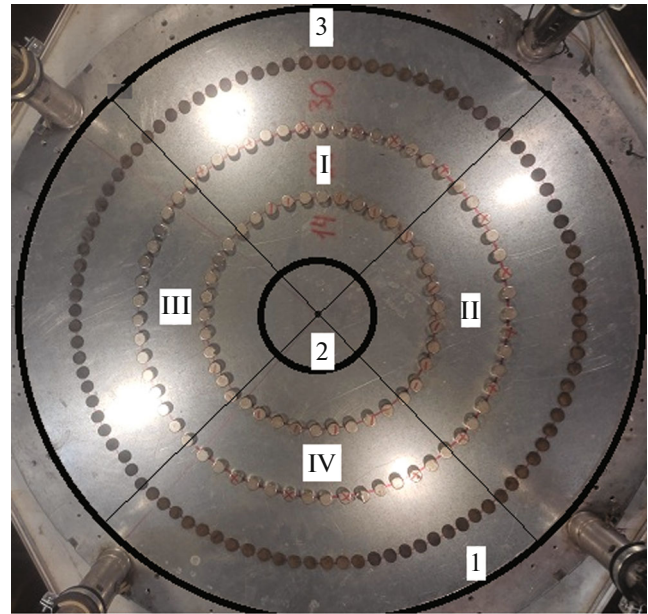In experiment 2, when the middle line of magnets was removed, only the western transport at midlati-

tudes and the eastern equatorial transport (trade winds) were modeled.

The difference between the source–sink method, which was used in numerical experiments (and laboratory experiments in (Gledzer et al., 2014)), and the MHD method is that sinks–sources induce currents due to the Coriolis force in a rotating channel, while in the MHD method the western and eastern transports are generated directly by the Ampère force.

Velocity anomalies in these flows in the experiments are formed by breaking the outer circular electrode 1 and electrode 3 isolated over a quarter of the circumference, to which a different current can be supplied than to electrode 1 (sector I in Fig. 7).

The velocity shear between the indicated multidirectional flows and the sloping bottom simulating the β effect form Rossby waves in the channel. Figures 8a ($T = 42.1$ s) and 8b ($T = 30.8$ s) show a sequence of images of flows in the channel (eddies and jets) at regular intervals $\left(\Delta\tau = \frac{10}{24}T\right)$. In the case shown in Fig. 8a, the currents at electrodes 1 and 3 were the same 400 mA, which is equivalent to solid electrode 1, and in Fig. 8b the current at electrode 3 was zero. The images closer to the center show three cyclonic eddies with a jet stream enveloping them. This entire triangular structure rotates counterclockwise, which indicates, similarly to the numerical experiments (Fig. 2), the westward motion of eddies, which is typical for Rossby waves (counterclockwise in the Southern Hemisphere).
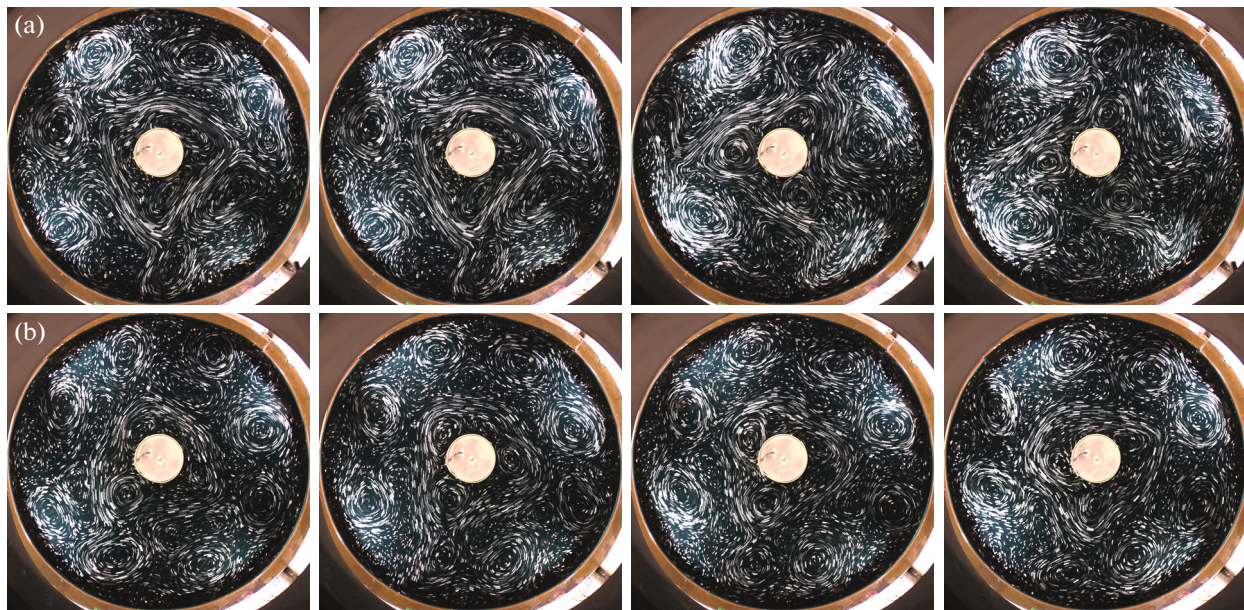
Fig. 8. Particle trajectories in the channel (images at regular time intervals $\Delta\tau = \frac{10}{24}T$) in the experiment: (a) at setup rotation period $T = 42.1$ s and current $j = 400$ mA at electrodes 1 and 3 (see Fig. 7); (b) at setup rotation period $T = 30.8$ s at current $j = 0$ at electrode 3 and current $j = 400$ mA at electrode 1. (a, b) Experiments with neodymium magnets on three circles.

A number of anticyclonic eddies formed near the outer boundary of the channel (equator), which slowly drifted to the western side (it can be seen from the four eddies in the upper part of the images in Fig. 8b or two clearly pronounced eddies on the left in Fig. 8a). At the bottom of the channel in Fig. 8b or on the right side in Fig. 8a, similarly to the numerical experiments in Fig. 2, the flow structure is not very regular: some anticyclones periodically disappear.

The results presented in Fig. 9 were obtained with an electric field anomaly in sector I: the current was switched off at electrode 3 (Fig. 7) ($j = 0$). At the same time, in sector I, the electric field was not equal to zero, since the current passes from electrode 1 to 2, occupying the entire space of sector I.

Figure 9a shows the mean vorticity over sectors I–IV (Fig. 7) (rotation period $T = 30.8$ s) at current $j = 400$ mA at electrode 1 and current $j = 0$ at electrode 3 (anomalous effect). For comparison, Fig. 9b shows the vorticity in sectors I–IV if the current at electrode 3 is $j = 400$ mA, i.e., in an unanomalous external influence. In addition to the strong dispersion of oscillations in the anomalous case, there is a clearly pronounced formation of time-averaged vorticities of opposite signs in sectors II and III following sector I. In sectors I (where an external anomaly of the electric field is introduced) and IV, in addition to the previously mentioned dispersion, the vorticity fluctuations are generally similar to the vorticity of anomalous circulation. In fact, due to the external anomaly in sector I,

the circulation in sector II becomes, on average, more anticyclonic, and in sector III, cyclonic.

Periodic oscillations shown in Fig. 9 with the characteristic time 60–80 s are reflected in the graphs in Fig. 9 showing the propagation of large eddies through sectors I–IV, similar to the eddies in the images of Fig. 8. It should be noted that the effect of the appearance of a nonzero mean vorticity in Figs. 9 in sectors II and III depends on the channel rotation period. In experiments with a long period $T = 42.4$ s, this effect becomes weakly pronounced.

Experiments were carried out with a different method of introducing an external anomaly into the flows in sector I. To do this, electrode 1 at the outer boundary of the channel remained solid, so the current j was supplied to the entire circular electrode at the boundary. However, the magnets in sector I were weaker than in the other parts in the remaining sectors (ferrite magnets). In this case, vertical component of the field was weaker in sector I, which led to a decrease in the Ampère force $\sim[\vec{j}, \vec{H}]$.

Figure 10 shows vorticity in sectors I–IV in the experiments in the described configuration at a current of 500 mA between electrodes 1 and 2 and a rotation period of $T = 21.2$ s. Here, vorticities in sectors I and IV generally behave synchronously, forming anticyclonic vorticity that propagates in sectors II and III: cyclonic average vorticity is generated, which also occupies a "hemisphere." It corresponds to the above-mentioned Rossby standing wave pattern with a wave number $m = 2$ (Fig. 2e).
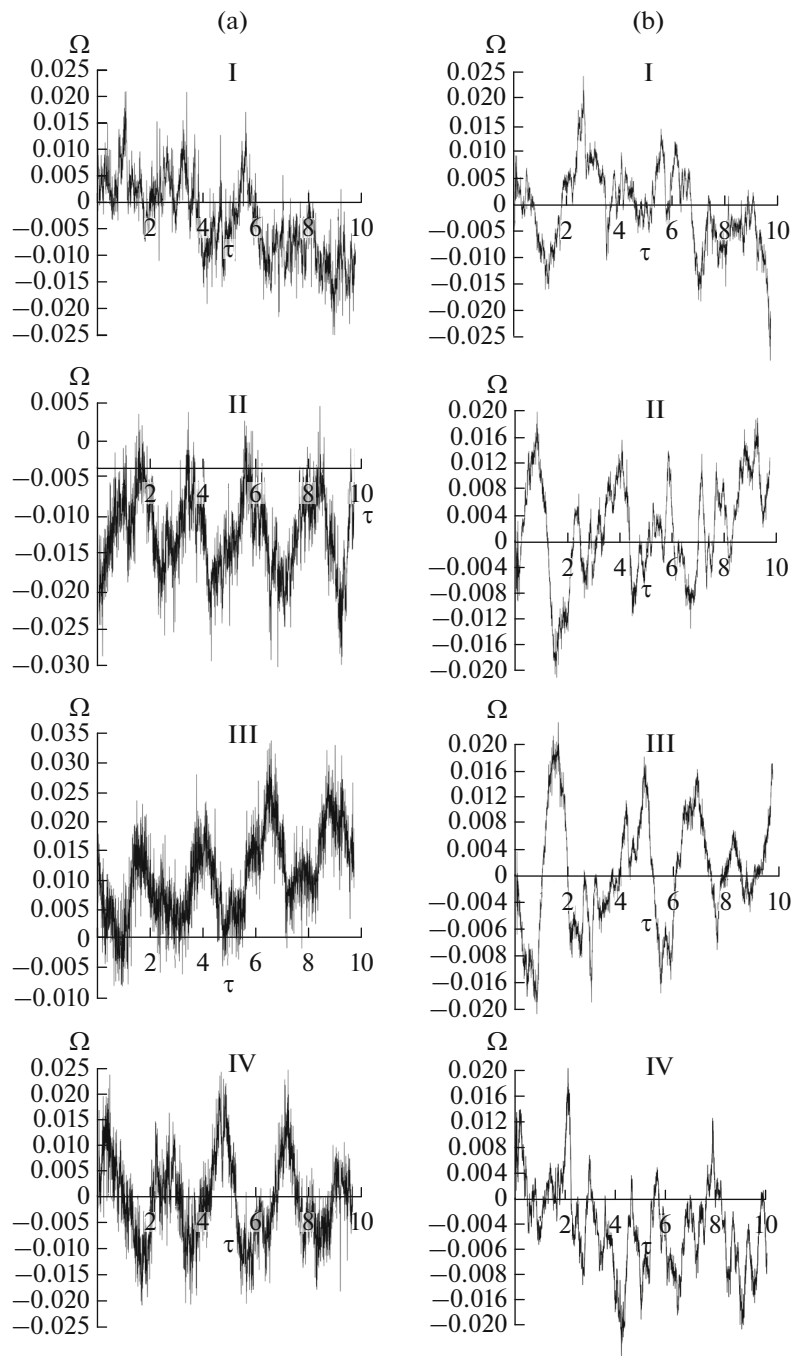
Fig. 9. Mean vorticities over sectors I−IV in the experiments: (a) with an anomalous effect of electric current and (b) without anomalous effect ($\tau = t/T$, $T = 30.8$ s).

Figure 11 shows time dependences of the angular coordinates of the centers of cyclones and anticyclones in the experiments with the same current $j = 400$ mA at electrodes 1 and 3 (a, b) and the anomalous action of the current (c, d and e, f), respectively; the $j = 300$ mA current at electrode 3 with current $j = 400$ mA at electrode 1, current $j = 100$ mA at electrode 3, and $j = 400$ mA at electrode 1 (experi-

ment 1). In the experiments, the results of which are shown in Fig. 11, the outer circle of magnets was removed; i.e., like in the numerical experiment in Fig. 5, a two-flow configuration has been implemented.

Figures 11a, 11c, and 11e show coordinates (τ, λ), $\tau = t/T$, $T = 29.2$ s of the cyclone centers in all previously described cases. At each moment there were
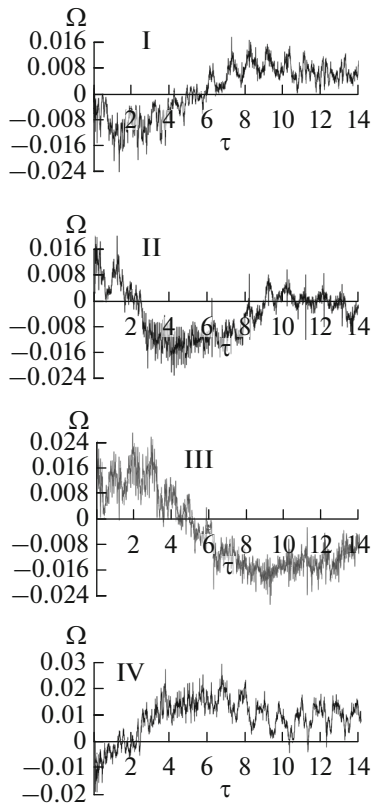
Fig. 10. Mean vorticities over sectors I–IV in an experiment with an anomalous arrangement of permanent magnets ($\tau = t/T$, $T = 21.2$ s).

three cyclones, which are seen in Fig. 8 in a triangular structure with an enveloping jet stream.

Four to five anticyclones are seen in the nonanomalous case (Fig. 11b) that move counterclockwise (increasing angle λ); this is a westward motion in the South Pole laboratory configuration. They move westward with almost the same speed along with the cyclones associated with them (Fig. 11a). Short-living anticyclones (marked by thin straight lines) are also seen in Fig. 11b, which almost do not move or slowly move eastward.

In the case of a weakly anomalous current distribution (Fig. 11d) at a current of $j = 300$ mA at electrode 3, westward moving anticyclones became less notable, but the number of short-living quasi-stationary anticyclones increased significantly (thin lines in Fig. 11d).

Under a strong anomaly in the current distribution ($j = 100$ mA at electrode 3) (Figs. 11e, 11f), the distribution of cyclones (Fig. 11e) in the plane (τ, λ) became more diffuse, but qualitatively close to the distributions in Figs. 11a and 11c.

A long-living (almost a week according to laboratory time) slowly moving eastward structure appeared in the distribution of anticyclones in the lower half of sector II (which in Fig. 11f corresponds to the angles $3\pi/2 < \lambda < 2\pi$).

The appearance of such structures was confirmed in experiment 2 (the middle line of magnets (Fig. 7) was removed). Figures 11aa and 11bb show the coordinates of the lines of anticyclone centers in the nonanomalous case (Fig. 11aa, $j = 400$ mA current at electrode 3) and in the case of a weak anomaly (Fig. 11bb) at a $j = 300$ mA current at electrode 3. In this case at $3\pi\,2 < \lambda < 2\pi$, several anticyclones developed at the bottom of sector II, which slowly drifted to the east.

It is interesting to compare the results of numerical and laboratory experiments on studying the dynamics of centers of cyclones and anticyclones with the corresponding data on atmospheric velocity fields. Figures 12a and 12b show the time dependences (months, from May (5) to October (10)) of the longitude of the centers (from 0° to 120° E) of cyclones (Fig. 12a) and anticyclones (Fig. 12b), which were located in latitude band from 35° to 65° N. The centers were determined by the previously described method based on the data on the velocity field at a level of 500 mb in 2010.

A region is notable in the cyclonic pattern in Fig. 12a (highlighted by an oval) between 40° and 60° E in the period from June (6) to September (9), in which there are almost no cyclones, which indicates a dry period in these months in the European part of the Russian Federation.

On the contrary, the lines of anticyclone centers condense during the same period of three months at longitudes from 80° to 100° E (anticyclones in Siberia, Kazakhstan, and Mongolia) and for almost a month (from August (8) to September (9)) at longitudes from 30° to 50° E. The center lines are almost horizontal, which corresponds to the quasi-stationary state of these anticyclones.

In other areas of the diagrams in Figs. 12a and 12b, cyclones and anticyclones show correlated motions to the east (tilts to the right of the vertical) under conditions of the westward transport of the general circulation of the atmosphere at midlatitudes. At the same time, there are no long periods of time during which the cyclones stop. In general, the diagrams in Figs. 12a and 12b are similar to Figs. 5c and 5d obtained numerically: the lifetime of cyclones and anticyclones in both cases is relatively short (up to a week in the atmosphere), which forms a discontinuous (broken) structure of center lines.

Diagrams in Figs. 12a and 12b, which show the anomalous 2010 for European Russia, can be compared with the same period in 2013. In this case, the cyclone lines almost uniformly fill the area of the diagram in Fig. 12c (from May (5) to October (10) and from 0° to 120° E), demonstrating the motion to the east. The diagram for anticyclones (Fig. 12d) shows a traditional region of almost not moving anticyclones between 80° and 100° E in the same months as in 2010. The region between 60° and 80° E, where the centers of anticyclones are absent, is distinguished; this region
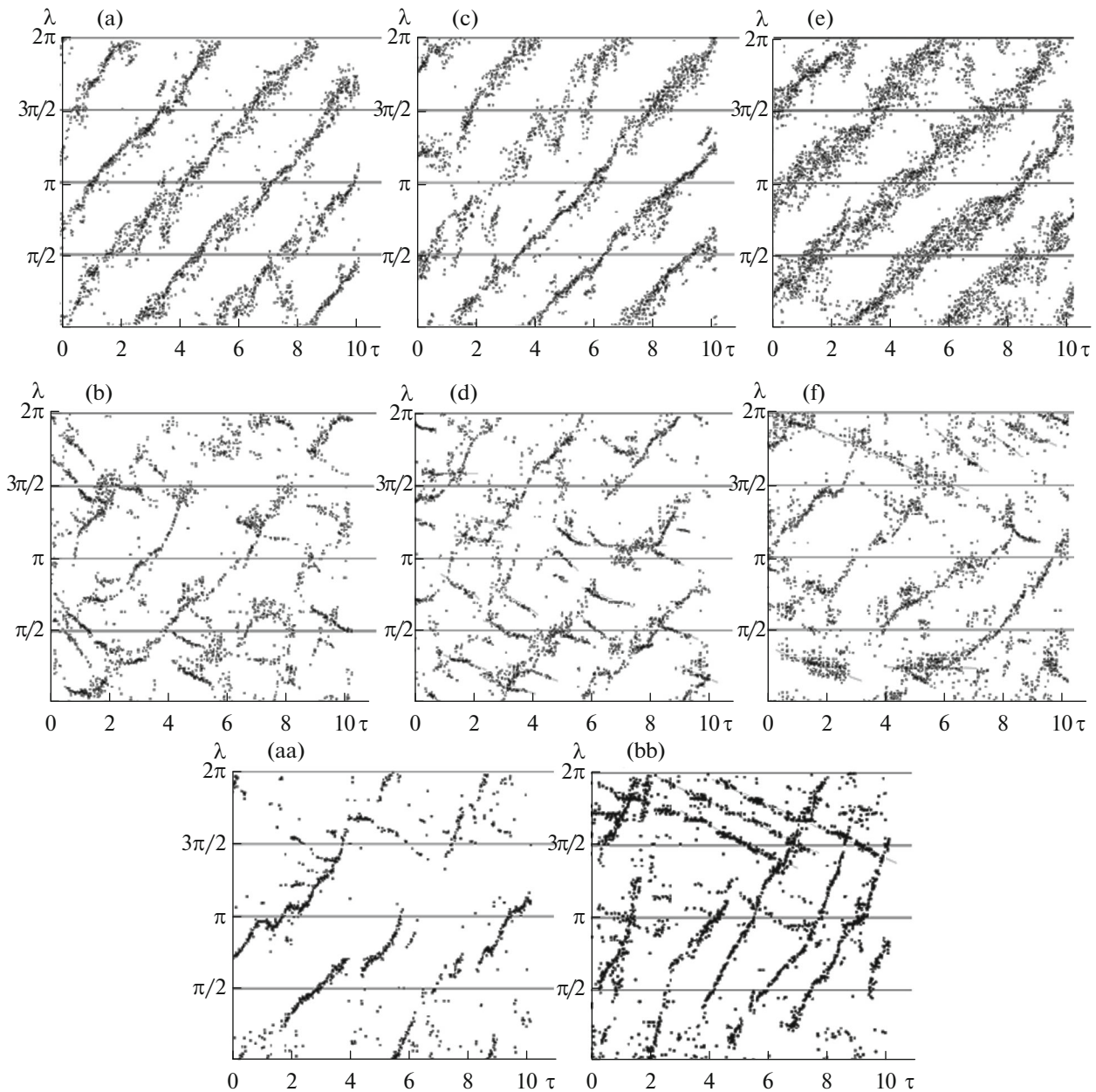
Fig. 11. Time evolution of $\tau = t/T$ ($T = 29.2$ s) of the azimuthal angular coordinates λ of the centers of cyclones (a, c, e) and anticyclones (b, d, f) in laboratory experiment 1: (a, b) with currents $j = 400$ mA at electrodes 1 and $j = 400$ mA on 3; (c, d) with currents $j = 400$ mA at electrode 1 and $j = 300$ mA at electrode 3; (e, f) with currents $j = 400$ mA at electrode 1 and $j = 100$ mA at electrode 3. Variations in centers of cyclones in experiment 2 ($T = 29.6$ s): (aa) with currents $j = 400$ mA at electrode 1 and $j = 400$ mA at electrode 3; (bb) with currents $j = 400$ mA at electrode 1 and $j = 300$ mA at electrode 3.

of the territory of the Russian Federation is occupied with propagating cyclones.

5. CONCLUSIONS

As was previously noted, symmetry breaking with respect to zonal spatial shears is necessary to reproduce stationary anomalies in the resonant interaction of transient modes in laboratory and numerical experiments. Such a violation can be compared with changes in the intensity of the subtropical Hadley cell, which, due to the rotation of the Earth, is associated with the cells of middle and polar latitudes.

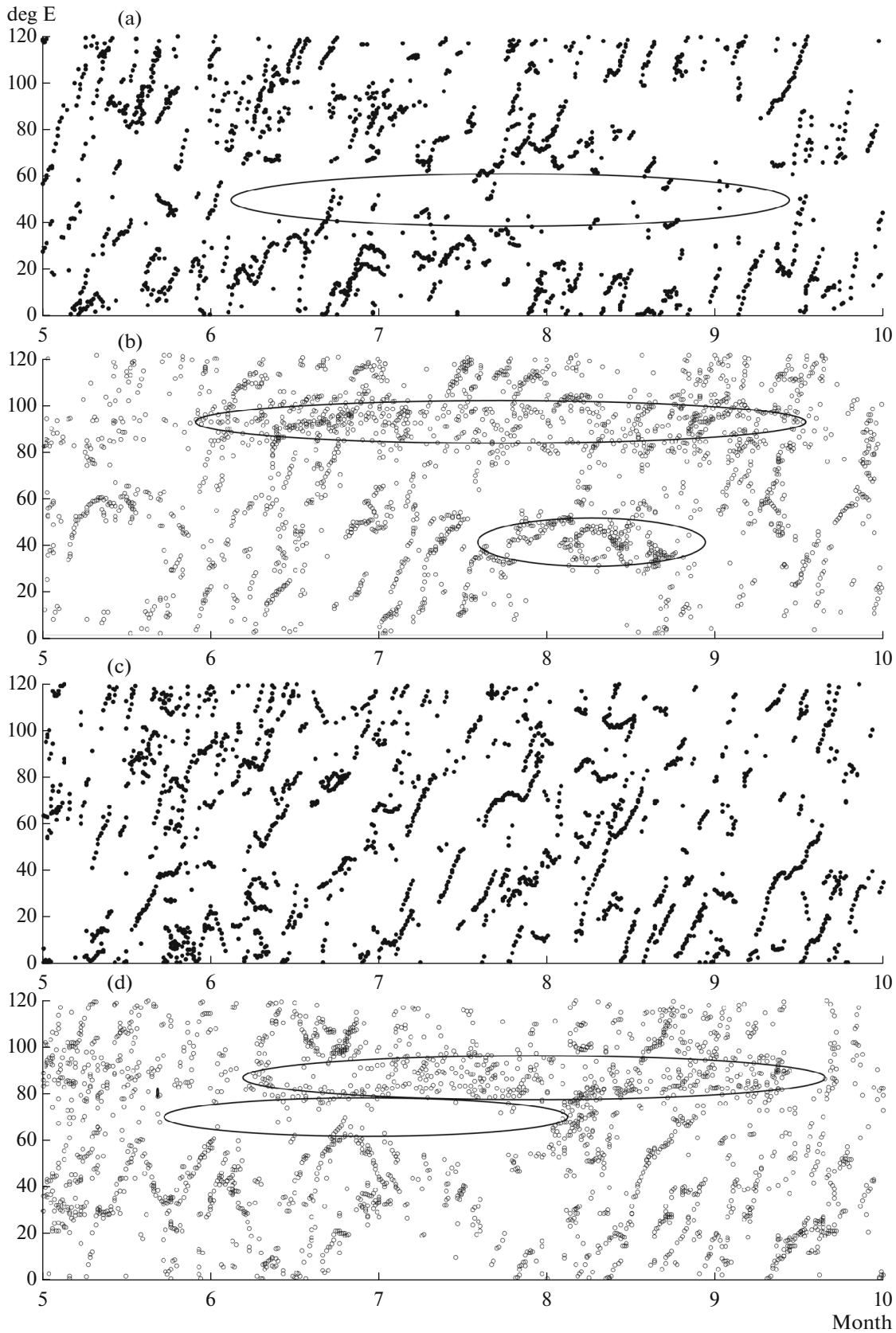Westward midlatitude transport in the troposphere is due to the Coriolis forcing when air moves from the

Fig. 12. Time dependence (months, from May (5) to October (10)) of the longitude of the centers (from 0° to 120° East longitude) of cyclones and anticyclones, which were located in the latitude band from 35° to 65° N: (a, b) in 2010; (c, d) in 2013.

tropics to the north (to the south in the Southern Hemisphere). This is the mean motion in the corresponding Farrel cell of the general atmospheric circulation. However, if the flow from the equatorial zone to high latitudes is disturbed (increased or weakened), the zonal western transport can change with a corresponding change in the cyclonic or anticyclonic activity at midlatitudes and in the polar cell with variations in the eastern transport in it.

In the numerical and laboratory experiments, anomalies in the flow were introduced by changing the intensity of sources—sinks or the Ampère force impact on the conducting fluid. At the same time, there were no notable changes in the visible pattern of eddy propagation in the channel in the sector in which external intervention was introduced (compare Fig. 8a ($T = 42.1$ s) and Fig. 8b ($T = 30.8$ s)). However, the results shown in Figs. 9 and 10 provide evidence that changes are notable in the mean characteristics of the eddy field when an anomaly is introduced; they are seen over the entire channel or its individual parts that do not belong to the sector with an external anomaly associated with an increase in the anticyclonic eddy component (dry periods) or cyclonic vorticity (wet periods).

The strongest influence of external force anomalies in numerical and laboratory experiments turned out to be the influence on the dynamics of anticyclones. A comparison of lines of anticyclone centers in Figs. 3b and 4c, 5b and 5d, and 11b and 11f shows that these anomalies have a decelerating effect on the velocity of propagation of anticyclones in the channel without almost affecting the dynamics of cyclones (Figs. 3a, 4b, 11a, 11c, 11e). At the same time, a significant part of moving anticyclones either disappears or almost stops (Figs. 11d, 11f), or new, quasi-stationary anticyclones appear (Fig. 11bb). However, they are not the source of blocking of the transport; they can be called "blocked" rather than "blocking" anticyclones.

Figures 3b, 4c, 11d, and 11f show that in numerical and laboratory experiments the angular velocity of anticyclones, if they move along the channel, is close to the angular velocity of the cyclones; i.e., together with cyclones, they form coupled structures of the dipole type. Quasi-stationary anticyclones form centers of action that prevent the free motion of such dipole formations.

Such a mixture of standing and moving eddies in a flow is similar to the background and transport circulation of waves in the resonant interaction of transient modes considered above, where, in addition to the stationary wave $\psi_0 = A_0 \cos(k_x x)$, there were waves transported with velocity $u_\pm = \dfrac{\omega \pm \nu}{k_x}$ with the same zonal wave number k_x.

REFERENCES

Antar, B.N. and Fowlis, W.W., Baroclinic instability of a rotating Hadley cell, *J. Atmos. Sci.*, 1981, vol. 38, pp. 2130−2141.

Chagelishvili, G.D. and Chkhetiani, O.G., Linear transformation of Rossby waves in shear flows, *Pis'ma Zh. Eksp. Teor. Fiz.*, 1995, vol. 62, no. 4, pp. 41−48.

Chkhetiani, O.G. and Kalashnik, M.V., Coupling blockings with transient instabilities, in *Intensivnye atmosfernye vikhri i ikh dinamika* (Intense Atmospheric Vortices and Their Dynamics), Mokhov, I.I., Kurganskii, M.V., and Chkhetiani, O.G., Eds., Moscow: Geos, 2018, pp. 189−199.

Chkhetiani, O.G., Kalashnik, M.V., and Chagelishvili, G.D., Dynamics and blocking of Rossby waves in quasi-two-dimensional shear flows, *JETP Lett.*, 2015, vol. 101, no. 2, pp. 79−84.

Cook, K.H., Role of continents in driving the Hadley cell, *J. Atmos. Sci.*, 2003, vol. 60, pp. 957−976.

Dolzhanskii, F.V., *Osnovy geofizicheskoi gidrodinamiki* (Fundamentals of Geophysical Hydrodynamics), Moscow: Fizmatlit, 2011.

Gledzer, A.E., Numerical model of currents generated by sources and sinks in a circular rotating channel, *Izv., Atmos. Ocean. Phys.*, 2014, vol. 50, no. 3, pp. 292−303.

Gledzer, A.E., Generation of large-scale structures and vortex systems in numerical experiments for rotating annular channels, *J. Appl. Mech. Tech. Phys.*, 2016, vol. 57, no. 7, pp. 1239−1253.

Gledzer, A.E., Gledzer, E.B., Khapaev, A.A., and Chkhetiani, O.G., Experimental manifestation of vortices and Rossby wave blocking at the MHD excitation of quasi-two-dimensional flows in a rotating cylindrical vessel, *JETP Lett.*, 2013, vol. 97, no. 6, pp. 316−321.

Gledzer, A.E., Gledzer, E.B., Khapaev, A.A., and Chernous'ko, Yu.L., Zonal flows, Rossby waves, and vortex transport in laboratory experiments with rotating annular channel, *Izv., Atmos. Ocean. Phys.*, 2014, vol. 50, no. 2, pp. 122−133.

Gledzer, A.E., Gledzer, E.B., Khapaev, A.A., Chkhetiani, O.G., and Shalimov, S.L., On the structures observed in thin rotating layers of a conductive fluid and the anomalies of the geomagnetic field, *Izv., Phys. Solid Earth*, 2018, vol. 54, no. 4, pp. 574−586.

Gledzer, A.E., Gledzer, E.B., Khapaev, A.A., and Chkhetiani, O.G., Multiplicity of flow regimes in thin fluid layers in rotating annular channels, *Fluid Dyn.*, 2021, vol. 56, no. 4, pp. 587−599.

Gledzer, E.B., Similarity parameters and a centrifugal convective instability of horizontally inhomogeneous circulations of the Hadley type, *Izv., Atmos. Ocean. Phys.* 2008, vol. 44, no. 1, pp. 33−44.

Gledzer, E.B. and Ponomarev, V.M., Instability of bounded flows with elliptical streamlines, *J. Fluid Mech.*, 1992, vol. 240, pp. 1−30.

Gledzer, E.B., Dolzhanskii, F.V., and Obukhov, A.M., *Sistemy gidrodinamicheskogo tipa i ikh primenenie* (Hydrodynamic-Type Systems and Their Application), Moscow: Nauka, 1981.

Lorentz, E.N., *The Nature and Theory of the General Circulation of the Atmosphere*, WMO, 1967; Leningrad: Gidrometeoizdat, 1970.

Matveev, L.T., *Fizika atmosfery* (Atmospheric Physics), St. Petersburg: Gidrometeoizdat, 2000.

Meshalkin, L.D. and Sinai, Ya.G., Investigation of the stability of a stationary solution of a system of equations of plane motion of an incompressible viscous fluid, *Prikl. Mat. Mekh.*, 1961, vol. 25, no. 6, pp. 1140−1143.

Mohanakumar, K., *Stratosphere Troposphere Interactions*, Springer, 2008; Moscow: Fizmatlit, 2011.

Obukhov, A.M., On the problem of geostrophic wind, *Izv. Akad. Nauk SSSR, Ser.: Geogr. Geofiz.*, 1949, vol. 13, no. 4, pp. 281−306.

Okeanologiya. Fizika Okeana (Oceanology. Physics of the Ocean), vol. 2: *Gidrodinamika okeana* (Hydrodynamics of the Ocean), Kamenkovich, V.M. and Monin, A.S., Eds., Moscow: Nauka, 1978.

Shukhman, I.G., Transient growth and optimal perturbations with the simplest dynamic model as an example, *Dokl. Phys.*, 2005, vol. 50, no. 6, pp. 308−310.

Sverdrup, H.U., Wind-driven currents in a baroclinic ocean; with application to the equatorial currents of the Eastern Pacific, *Proc. Natl. Acad. Sci. U. S. A.*, 1947, vol. 33, no. 11, pp. 318−326.

Translated by E. Morozov